In summary, the qualitative model is consistent with the following assumptions: (1) Single-ion magnetic moments lie essentially in the x–y plane defined by the coordinate system of the EFG, i.e., $^5B_{2g}$ (d_{xy}) electronic ground state. (2) Isotropic superexchange aligns the spins antiparallel along the chain or c axis. (3) Anisotropic superexchange occurs along the chain and results in a weak net spontaneous (D–M) moment directed parallel to the crystallographic a cell axis (in accordance with Moriya's rules). (4) A sharp saturation in the superexchange ordering below T_c (as seen in the magnetic susceptibility and Mössbauer spectra) indicates the Ising behavior of the Fe(II) ion. (5) Interchain interactions are not predicted to occur until $T \rightarrow 0$ K. From these results we conclude that the iron hippurate molecule represents the first example of a one-dimensional Ising chain system for which magnetic ordering in the second and third dimensions is not predicted to occur until $T \rightarrow 0$ K.

These studies indicate the utility of providing new series of molecular systems whose properties can be used to evaluate existing theoretical models. Furthermore, an understanding of the relationship between structure and magnetic properties can be used in the strategic synthesis of new magnetic systems for practical applications.

Acknowledgment. The authors wish to thank Dr. W. M. Reiff for use of the variable-temperature Mössbauer equipment in his laboratory and for the computer analysis of the collected Mössbauer data. The authors are also grateful to Dr. O. F. Griffith for valuable discussions on dipole–dipole magnetic interactions. Partial funding for this work was provided by NSF Grant No. CHE-76-17434-A03.

Registry No. $Fe(hipp)_2(H_2O)_3 \cdot 2H_2O$, 75180-59-5.

Contribution from the Laboratoire de Spectrochimie des Elêments de Transition, ERA No. 672, Université de Paris-Sud, 91405 Orsay, France, and the Laboratoire de Chimie de Coordination, Associé à l'Université Paul Sabatier, 31030 Toulouse, France

Crystal Structure and Magnetic and EPR Properties of the Heterobinuclear Complex $CuNi(fsa)_2en(H_2O)_2 \cdot H_2O$ ($H_4(fsa)_2en$ = *N,N'*-Bis(2-hydroxy-3-carboxybenzylidene)-1,2-diaminoethane)

I. MORGENSTERN-BADARAU,*[1a] M. RERAT,[1a] O. KAHN,*[1a] J. JAUD,[1b] and J. GALY*[1b]

Received November 3, 1981

The goal of this paper is to investigate the exchange interaction in $CuNi(fsa)_2en(H_2O)_2 \cdot H_2O$, denoted [CuNi], where $(fsa)_2en^{4-}$ is the bichelating ligand derived from the Schiff base *N,N'*-(1-hydroxy-2-carboxybenzylidene)-1,2-diaminoethane. For a comparison of the structure of the pair states in [CuNi] with those of Cu(II) and Ni(II) single-ion ground states, $CuMg(fsa)_2en(H_2O)_2 \cdot H_2O$ and $Ni_2(fsa)_2en(H_2O)_2 \cdot H_2O$, denoted [CuMg] and [NiNi], have also been investigated. The crystal structure of [CuNi] has been solved at −120 °C from 8428 reflections. [CuNi] crystallizes in the trigonal system, space group $P3_1$. The lattice constants are a = 12.8071 (4) Å and c = 9.8157 (8) Å with Z = 3. The structure is made of [CuNi] binuclear units, in which the copper atom is in a strictly planar $-N_2O_2$ environment and the nickel atom in a pseudooctahedral $-O_2O_2(H_2O)_2$ environment. The crystal structure of [NiNi] has been solved at room temperature from 3262 reflections. The space group is $P3_2$, and the structure of the binuclear units [NiNi] is very close to that of the units [CuNi]. The temperature dependence of the magnetic susceptibility of [CuNi], studied in the temperature range 4–300 K, has revealed an energy gap of $-3J/2$ = 213 cm^{-1} between the $^2A_1$ ground state and the $^4A_1$ excited state. The average values of the g factors for the two pair states have been compared to those of the single ions, as deduced from the magnetic behavior of [CuMg] and [NiNi]. The EPR powder spectrum of [CuNi] is typical of an axial symmetry. The single-crystal spectra at 4 K exhibit only one signal for any orientation, assigned to the ground-pair doublet state. The **g** tensor is axial with the unique axis perpendicular to the $N_2CuO_2NiO_2$ pseudo molecular plane. The principal values are $g_\parallel$ = 2.22 (5) and $g_\perp$ = 2.30 (0). The signal broadens out against the temperature in an inhomogeneous manner, the broadening being more pronounced on the high-field side. The magnetic and the EPR data are compared. The *status* of the spin Hamiltonian utilized to interpret these data is discussed. Finally, the mechanism of the exchange interaction is specified. The existence of two exchange pathways, namely, $J_{b_1b_1}$ and $J_{b_1a_1}$, the former being antiferromagnetic and the latter ferromagnetic, is emphasized.

Introduction

If a large interest continues to be taken in the binuclear complexes with identical paramagnetic metallic ions, an evolution started half a decade ago toward the heterobimetallic complexes. Significant theoretical progress concerning the mechanism of the interaction was achieved owing to the study of such compounds;[2,3] much more may be expected.

This field of the heterbinuclear complexes with paramagnetic centers if still limited today by the small number of known and fully structurally characterized compounds and by the relative difficulty of synthesizing new compounds.[4] Probably, it is one of the reasons why some groups focus on doped systems,[5-10] for instance, a few percent of Ni^{2+} in a $[Cu^{II}Cu^{II}]$ matrix or a few percent of Cu^{2+} in a $[Ni^{II}Ni^{II}]$ matrix. The EPR is then a quite appropriate technique to investigate the very low-lying states in the $[Cu^{II}Ni^{II}]$ pairs. Moreover, the magnetic dilution often enables the observation of hyperfine structure, which can itself provide information

(1) (a) Université de Paris-Sud. (b) Université Paul Sabatier.
(2) Kahn, O.; Galy, J.; Journaux, Y.; Jaud, J.; Morgenstern-Badarau, I. *J. Am. Chem. Soc.* **1982**, *104*, 2165.
(3) Journaux, Y.; Coudanne, H.; Kahn, O. *Angew. Chem., Int. Ed. Engl.*, in press.
(4) Casellato, U.; Vigato, P. A.; Fenton, D. E.; Vidali, M. *Chem. Soc. Rev.* **1979**, *8*, 199 and references therein.
(5) Paulson, J. A.; Krost, D. A.; McPherson, G. L.; Rogers, R. D.; Atwood, J. L. *Inorg. Chem.* **1980**, *19*, 2519.
(6) Banci, L.; Bencini, A.; Dei, A.; Gatteschi, D. *Inorg. Chem.* **1981**, *20*, 393.
(7) Buluggiu, E. *J. Phys. Chem. Solids* **1980**, *41*, 43, 1175.
(8) Banci, L.; Bencini, A.; Benelli, C.; Dei, A.; Gatteschi, D. *Inorg. Chem.* **1981**, *20*, 1399.
(9) Kokoszka, G. E.; Allen, H. C., Jr.; Gordon, G. *J. Chem. Phys.* **1967**, *46*, 3020.
(10) Banci, L.; Bencini, A.; Gatteschi, D. *Inorg. Chem.* **1981**, *20*, 2734.

0020-1669/82/1321-3050$01.25/0

on the interaction between metallic centers.[5-10] However, in such systems, it is most difficult to determine accurately the energy gaps between the low-lying states. Indeed, the study of the temperature dependence of the EPR signals is generally very tedious and even may be impossible when the host lattice itself has a magnetic excited state close to the ground state. The difficulty in the determination of these energy gaps is a severe limitation, since they are directly related to the isotropic exchange parameter, which is by far the leading term of the exchange. This difficulty disappears when one works on pure heterobinuclear complexes. In this case, magnetic susceptibility measurements carried out with the high-sensitivity magnetometers now available can lead to a rather accurate determination of the isotropic exchange parameters,[11,12] especially when the interaction gives rise to only two spin states, as in the $Cu^{II}Ni^{II}$ pair. On the other hand, the magnetic susceptibility technique is not adapted to the study of the fine structures of these spin states. Therefore, there is a complementarity between the two techniques, magnetism and EPR, already largely utilized in the study of the homobinuclear complexes[13,14] but curiously, until now, very rarely utilized in the field of the heterobinuclear complexes.

In this paper, we investigate the interaction in $CuNi(fsa)_2en(H_2O)_2 \cdot H_2O$, denoted [CuNi], where $(fsa)_2en^{4-}$ is the bichelating ligand derived from the Schiff base *N,N'*-(1-hydroxy-2-carboxybenzylidene)-1,2-diaminoethane. In order to see to what extent the electronic structure of [CuNi] may be deduced from those of Cu^{II} and Ni^{II} single-ion ground states, we shall also investigate the complexes $CuMg(fsa)_2en(H_2O)_2 \cdot H_2O$[15] and $Ni_2(fsa)_2en(H_2O)_2 \cdot H_2O$,[16] denoted [CuMg] and [NiNi], respectively. The crystal structure of [CuMg] was known;[15] we determined those of [CuNi] and [NiNi]. [CuMg] and [CuNi] are isomorphous, and the Cu^{II} ions in both complexes occupy the same $-N_2O_2$ inside site. [NiNi] is not strictly isomorphous to [CuNi]; however, the crystal lattices and the molecular symmetries are very close. In [NiNi], only the Ni^{II} ion occupying the outside site, in the $-O_2O_2(H_2O)_2$ pseudooctahedral surrounding, is magnetic.[16]

Experimental Section

[CuMg], [NiNi], and [CuNi] were synthesized as described in ref 15. [NiNi] was directly obtained as single crystals suitable for X-ray study. Crystals of [CuNi] suitable for both X-ray study and EPR were obtained by very slow evaporation of a methanolic solution.

Crystal Structure and Refinement. Crystals of [NiNi] and [CuNi] were selected and studied by X-ray photographic methods using Explorer and Weissenberg cameras (Zr-filled Mo Kα and Ni-filtered Cu Kα radiation). Approximate unit cell parameters and possible space groups were derived from photographic data sets. Both complexes crystallize in the trigonal system. Laue diagrams and the various precession and Weissenberg photographs exhibiting the systematic absence of reflections 00*l* with $l \neq 3n$ indicate the possible space groups $P3_121$ or $P3_221$ (Laue group $\bar{3}m1$) or $P3_1$ or $P3_2$ (Laue group $\bar{3}$).

Space Group Problem. The X-ray powder spectra of [CuCo], [CuMg], and [CuNi] strongly suggest that the three compounds are isomorphous. According to Mikuriya et al.,[19] the crystal structure of [CuCo] belongs to the Laue group $\bar{3}m1$ and the structure admits the space group $P3_221$. According to Beale et al.,[15] [CuMg] belongs to the same Laue group but with the space group $P3_121$. Therefore, it was necessary, for the determination of the correct space group for the series, to make an accurate X-ray analysis of the intensity of the various reflections *hkl*. This analysis was carried out on [CuNi] at −120 °C; from a complete full-reflection-sphere analysis up to a θ angle of 30°, it clearly appeared that the intensity relations between *hkl* reflections were $I(hkl) = I(\bar{h}\bar{k}l) = I(kil) \neq (\bar{h}kl) \neq I(i\bar{k}l) \neq I(hk\bar{l}) \neq I(khl)$,[20] implying with the systematic absences noted above the two possible space groups $P3_1$ and $P3_2$. This result is rather different from those obtained with [CuCo][19] and [CuMg].[15] Indeed, it indicates that the intramolecular Cu–M axis is not a genuine crystallographic twofold axis.

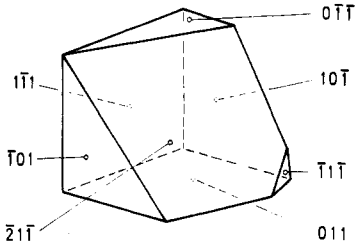

Figure 1. Morphology of the crystal of [CuNi] on which the absorption corrections were numerically calculated.

Data Collection. The crysals of [CuNi] and [NiNi] were mounted on a CAD-4 Enraf-Nonius PDP8/M computer-controlled single-crystal diffractometer, and the unit cells were refined by optimizing the settings of 25 reflections (Mo Kα radiation). The results are shown in Table I, as well as the schedule for the measurement of the intensity of the reflections. The reflections were corrected for Lorentz and polarization factors; spherical absorption corrections were applied to the [NiNi] crystal, and numerical absorption corrections were calculated for the [CuNi] crystal whose exact shape and face indexing were analyzed, as shown in Figure 1. In this latter case, the intensities of the utilized set of *khl* reflections were obtained by averaging the intensities of the equivalent reflections. Atomic scattering factors of Cromer and Waber for the nonhydrogen atoms[21] and those of Stewart, Davidson, and Simpson for the spherical hydrogen atoms[22] were used. Real and imaginary dispersion corrections given by Cromer were applied for copper and nickel atoms.[23] The first calculations were performed by using the coordinates published by Mikuriya[19] for the heavy atoms and their nearest-neighbor oxygen and nitrogen atoms. Then, by Fourier synthesis, it was possible to locate the remaining oxygen and carbon atoms. The structures were then refined by full-matrix least-squares techniques. Difference Fourier maps and a priori calculations made it possible for the positions of the hydrogen atoms to be determined. All nonhydrogen atoms were then allowed to refine with anisotropic thermal parameters and a fixed isotropic thermal parameter of $B_H = 1.2B_{eq}(C)$ Å^2 was used for hydrogen atoms ($B_{eq}(C)$ is the isotropic equivalent factor of the carbon to which the hydrogen is bound; $B_{eq}(C) = {}^4/_3\sum_{i,j}((\vec{a}_i \cdot \vec{a}_j)\beta_{ij})$. In both structures, the last difference Fourier maps then showed no peak greater than 0.2 e Å^{-3}, even around the oxygen atoms of the water molecules where the hydrogen atoms were not located. It must be pointed out here that our structure analysis gave a correlation matrix showing clearly that the molecules do not adopt a genuine twofold axis, confirming the choice of the space groups $P3_1$ for [CuNi] and $P3_2$ for [NiNi].

Magnetism. The magnetic measurements were carried out on polycrystalline samples weighing about 8 mg in the temperature range 3.8–300 K with a Faraday type magnetometer equipped with an Oxford Instruments continuous-flow cryostat. The independence of susceptibility against the magnetic field was checked at room temperature and also at 20 and 4.2 K for [CuNi]. Tetrakis(thiocyanato)mercury cobaltate was used as a susceptibility standard. For the compounds, the diamagnetism was estimated as -240×10^{-6} cm^3 mol^{-1}. This value is that of the magnetic susceptibility of $NiCd(fsa)_2en \cdot 3.5H_2O$, in which the two metallic ions are diamagnetic. The

(11) O'Connor, C. J.; Freyberg, D. P.; Sinn, E. *Inorg. Chem.* **1979**, *18*, 1077.
(12) Jaud, J.; Journaux, Y.; Galy, J.; Kahn, O. *Nouv. J. Chim.* **1980**, *4*, 629.
(13) See, for instance: Corbin, D. R.; Francesconi, L. C.; Hendrickson, D. N.; Stucky, G. D. *Inorg. Chem.* **1981**, *20*, 2084 and references therein.
(14) Comarmond, J.; Lehn, J. M.; Plumere, P.; Agnus, Y.; Louis, R.; Weiss, R.; Kahn, O.; Morgenstern-Badarau, I. *J. Am. Chem. Soc.*, in press.
(15) Beale, J. P.; Cunningham, J. A.; Phillips, D. J. *Inorg. Chim. Acta* **1979**, *33*, 113.
(16) Tanaka, M.; Kitaoka, M.; Okawa, H.; Kida, S. *Bull. Chem. Soc. Jpn.* **1976**, *49*, 2469.
(17) Okawa, H.; Tanaka, M.; Kida, S. *Chem. Lett.* **1974**, 987.
(18) Torihara, N.; Okawa, H.; Kida, S. *Inorg. Chim. Acta* **1976**, *26*, 97.
(19) Mikuriya, M.; Okawa, H.; Kida, S.; Ueda, I. *Bull. Chem. Soc. Jpn.* **1978**, *51*, 2920.
(20) "International Tables for X-ray Crystallography"; Kynoch Press: Birmingham, England, 1969; Vol. 1, p 462.
(21) Cromer, D. T.; Waber, J. T. *Acta Crystallogr.* **1965**, *18*, 104.
(22) Stewart, R. F.; Davidson, E. R.; Simpson, W. T. *J. Chem. Phys.* **1965**, *42*, 3175.
(23) Cromer, D. T. *J. Chem. Phys.* **1969**, *50*, 4857.

Table I. Information Concerning the Crystallographic Data Collections for [NiNi] and [CuNi]

	$Ni_2O_8N_2C_{18}H_{15}\cdot H_2O$	$CuNiO_8N_2C_{18}H_{15}\cdot H_2O$
	Crystallographic and Physical Data	
cryst syst	trigonal	trigonal
a, Å	12.7701 (8)	12.8071 (4)
c, Å	9.9409 (17)	9.8157 (8)
mol wt	523.623	528.459
space group	$P3_2$	$P3_1$
V, Å	1403.9 (6)	1394.3 (2)
Z	3	3
$F(000)$	792	795
ρ_X, g cm^{-3}	1.844	1.874
abs factor, cm^{-1}	20.7	22.6
morphology	little regular block, max and min size (mm) 0.28, 0.24	Figure 1
	Data Collection	
temp, °C	21	−120
radiation	Mo Kα	
monochromatization	graphite monochromator	
λ(Kα)	0.71069	
cryst–detector distn, mm	207	
detector window height and width, mm	4, 4	
takeoff angle, deg	3.5	3.4
scan angle for ω angle, deg	0.70 + 0.347 tan θ	0.65 + 0.347 tan θ
scan mode	0–2θ	
max Bragg angle, deg	30	52
values determining scan speed		
SIGPRE	0.700	0.750
SIGMA	0.018	0.008
VPRE, deg min^{-1}	10	5
TMAX, s	80	120
control reflctns		
intens, periodicity 3600 s	$\bar{9}00$, 090, $9\bar{3}2$	$\bar{4}9\bar{2}$, $\underline{9}00$, $70\bar{1}$, $0\bar{9}0$
orientation after 100 reflctns	1,10,4, 392, 394	$8\bar{2}0$, $\bar{1}$,1,0,2, 10,$\bar{1}$,$\bar{4}$
	Conditions for Refinement	
reflctns for the refinement of the cell dimens	25	25
recorded reflctns	4528	9384
utilized reflctns	3262 ($I > \sigma(I)$)	8428
refined parameters	288	288
reliability factors		
$R = \Sigma \lvert kF_o - \lvert F_c \rvert \rvert / \Sigma kF_o$	0.0362	0.0392
$R_w = [\Sigma w(kF_o - F_c)^2/(NO - NV)]^{1/2}$	1.2148	1.1157

uncertainty of the temperature is 0.1 K, and the reproducibility of the magnetic susceptibilities for different samples of the same compound is 1%.

EPR. The spectra were recorded at X-band frequency with a Bruker ER 200 D spectrometer equipped with an Oxford Instruments continuous-flow cryostat. A 100-kHz field modulation was used. The magnetic field was determined with a Hall probe and the klystron frequency with a Hewlett-Packard frequency meter. Powder, single-crystal, and glass samples were studied. Crystals were orientated in the magnetic field with respect to the principal crystal axis. Glasses were obtained from 90% methanol–10% ethanol solutions.

Results and Discussion of the Structures

Atomic coordinates and anisotropic temperature factors are given in part a of Table II for [NiNi] and part b for [CuNi].[24] The interatomic distances and the bond angles are listed in Table III. The asymmeric unit cell contains one MNi(fsa)$_2$en(H$_2$O)$_2$ molecule with M = Ni or Cu and one nonbound water molecule disordered on two crystallographic positions with 50% occupancy. The perspective view of CuNi(fsa)$_2$en(H$_2$O)·H$_2$O is given in Figure 2, with the already described labeling.[25]

Concerning the ligand part of the complexes, the bond lengths and bond angles are in good agreement with the previous structural investigations of similar complexes.[2,15,16,19,25] In both structures, the metallic ion occupying the inside site exhibits a strict square-planar environment; the deviation of M from the mean plane O(1)O(2)N(5)N(6) is less than 0.03

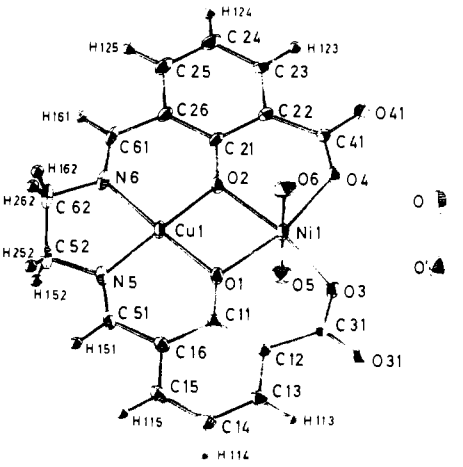

Figure 2. Perspective view of CuNi(fsa)$_2$en(H$_2$O)$_2$·H$_2$O.

Å for M = Cu and 0.003 Å for M = Ni (see Table IV). The same situation holds in CuCo(fsa)$_2$en(H$_2$O)$_2$·H$_2$O, denoted [CuCo],[19] in CuCo(fsa)$_2$en(H$_2$O)·5H$_2$O of orthorhombic symmetry,[25] and in [CuMg].[15] In contrast, in CuM′(fsa)$_2$en·CH$_3$OH with M′ = Cu or VO,[2,26] the presence of a weakly bound methanol molecule pulls the copper atom out of the mean plane by more than 0.20 Å. The Ni(II) ion occupying the outside site exhibits a pseudooctahedral coordination. The equatorial Ni–O bonds are equal within ±0.01 Å, and the axial distances Ni–O corresponding to the bonds

(24) The refinement for [CuNi] was performed on the reflections with $I \geq 4\sigma(I)$, i.e., 8428 *hkl*, to limit the computation cost.
(25) Galy, J.; Jaud, J.; Kahn, O.; Tola, P. *Inorg. Chem.* **1980**, *19*, 2945.
(26) Galy, J.; Jaud, J.; Kahn, O.; Tola, P. *Inorg. Chim. Acta* **1979**, *36*, 229.

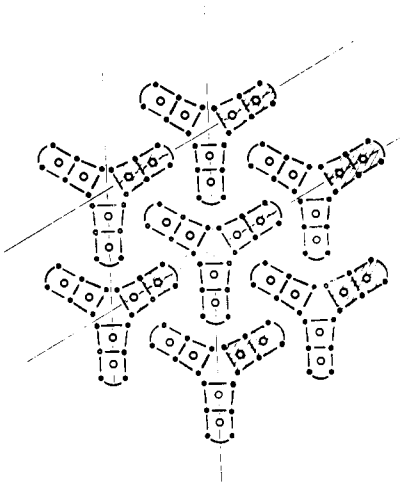

Figure 3. Schematic representation of the packing in [CuNi].

Ni–(water molecule) are elongated as usually observed.

The absence of intramolecular direct interaction in [CuNi] is indicated by the short interatomic distance O(1)–O(2) (2.541 (3) Å) and the correlative pinching of the O(1)Ni(1)O(2) angle (77.9 (1)°). This angle is smaller than the O(1)Cu(1)O(2) angle (84.2 (1)°), owing to the more rigid environment of the inside site. It turns out that the nickel atom in the outside site is repulsed toward the O(3)–O(4) axis. This leads to a large O(3)Ni(1)O(4) angle (103.8 (1)°) and a large O(3)–O(4) distance (3.128 (3) Å). Mikuriya et al.[19] and Beale et al.[15] even found larger values for the O(3)M′O(4) angle (110.7 (2)° in [CuCo] and 110.8 (1)° in [CuMg]). Such surprisingly large values have to be related with the constraints imposed by the presence of a twofold axis in the space groups retained by these authors, $P3_221$ and $P3_121$, respectively. All the comments made above on the outside site in [CuNi] hold for [NiNi].

Up to now, the structures of four $MM'(fsa)_2en(H_2O)_2 \cdot H_2O$ complexes crystallizing in the trigonal system were described, namely, [CuCo], [CuMg], [NiNi], and [CuNi]. In spite of the results already presented for the first two complexes, our opinion is that none of them adopts a genuine crystallographic twofold axis. We have then two families: [CuMg] and [CuNi] on the one hand, crystallizing in the $P3_1$ space group, and [CuCo] and [NiNi] on the other hand, crystallizing in the $P3_2$ space group. For the former family, the molecules are piled up counterclockwise along the z crystallographic direction; for the latter family, they are piled up clockwise. The reasons why these two families exist are not clear to us. Without drawing any conclusion on this, we may notice that in one family the complexes have an odd number of unpaired electrons while in the other one they have an even number of unpaired electrons. The packing of the structure of [CuNi] is schematized in Figure 3. One can notice that the pseudo molecular planes $N_2CuO_2NiO_2$ are nearly perpendicular to the c axis.

Magnetic Properties. We idealized somewhat the molecular structure of the three complexes [CuMg], [NiNi], and [CuNi] by assuming a C_{2v} symmetry for each of the metallic sites and for the whole molecule. The actual symmetry is in fact very close to C_{2v}. The reference used is shown by I, where the z molecular axis is almost parallel to the c crystal axis.

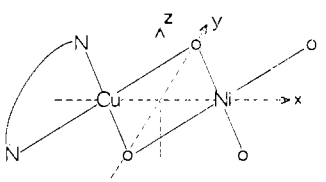

I

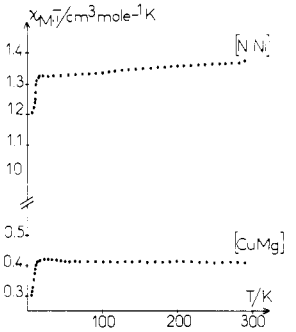

Figure 4. Temperature dependence of $\chi_M T$ for [CuMg] and [CuNi].

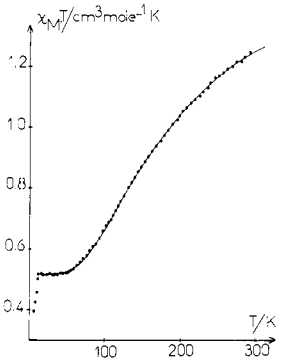

Figure 5. Experimental (●) and theoretical (—) temperature dependence of $\chi_M T$ for [CuNi].

In [CuMg], only the Cu^{II} ion is magnetic. Its ground state is $^2B_1$. The magnetic behavior is shown in Figure 4, in the form of the variation against temperature of the product $\chi_M T$ of the molar magnetic susceptibility vs. the temperature. It follows a Curie law between 300 and 20 K. Around 20 K where the effect of the corrections of diamagnetism and of TIP is minimized, we have $\chi_M T = 0.41$ (8) cm^3 mol^{-1} K, corresponding to $\tilde{g}_{Cu} = 2.11$ for the average value of the g_{Cu} factor ($\chi_M T = N\beta^2 \tilde{g}_{Cu}^2/4k$). Below 20 K, $\chi_M T$ decreases down to 0.31 cm^3 mol^{-1} K at 4.2 K, due most likely to a very weak intermolecular antiferromagnetic coupling.

In [NiNi], the inside Ni^{II} ion in the $-N_2O_2$ square surrounding is diamagnetic, so that the observed magnetic properties are those of the outside Ni^{II} in a pseudooctahedral environment with a $^3B_1$ ground state. The magnetic behavior is shown in Figure 4. In the 300–18 K temperature range, $\chi_M T$ linearly decreases with a very weak slope. The magnetic data closely follow the relation

$$\chi_M T/\text{cm}^3\ \text{mol}^{-1}\ \text{K} = 1.31\ (7) + (220 \times 10^{-6})T/\text{K}$$

The value 220×10^{-6} cm^3 mol^{-1} is quite reasonable for the TIP of two Ni^{II} ions. The Curie constant 1.31 (7) cm^3 mol^{-1} K corresponds to $\tilde{g}_{Ni} = 2.29$ for the average value of the g_{Ni} factor ($\chi_M T = 2N\beta^2 \tilde{g}_{Ni}^2/3k$). Below 18 K, $\chi_M T$ decreases more rapidly down to 1.1 cm^3 mol^{-1} K at 4.2 K. Again, this behavior at very low temperature is likely due to a weak intermolecular antiferromagnetic interaction. The zero-field splitting of the $^3B_1$ state, put in evidence by the absence of an EPR signal (see below) may also contribute to the decrease of $\chi_M T$ below 18 K.

The magnetic results for [CuMg] and [NiNi] show that, above 20 K, the magnetic behavior of these systems can be interpreted without considering intermolecular effects.

In [CuNi], both transition ions are magnetic and the interaction between the $^2B_1$ single-ion ground state for Cu^{II} and the $^3B_1$ single-ion ground state for Ni^{II} leads to the two molecular states $^2A_1$ and $^4A_1$. This latter state may be split into two Kramers doublets by the zero-field splitting. The temperature dependence of $\chi_M T$ is shown in Figure 5. This study

Table II. Atomic Coordinates and Thermal Factors for [NiNi] and [CuNi][a]

(a) [NiNi]

atom	x	y	z	B_{11}	B_{22}	B_{33}	B_{12}	B_{13}	B_{23}
Ni(2)	0.45143 (5)	0.45154 (5)	0	2.82 (4)	2.83 (4)	6.09 (5)	0.39 (5)	−0.30 (4)	0.33 (4)
Ni(1)	0.21972 (4)	0.21976 (4)	0.00014 (8)	2.45 (3)	2.43 (3)	7.28 (6)	1.15 (3)	−0.17 (4)	0.16 (4)
O(1)	0.3996 (3)	0.2874 (3)	−0.0036 (4)	1.5 (2)	2.5 (2)	8.7 (4)	0.7 (2)	−0.2 (2)	−0.1 (2)
O(2)	0.2877 (3)	0.3998 (3)	0.0029 (4)	2.5 (2)	1.7 (2)	8.6 (4)	0.8 (2)	−0.1 (2)	0.3 (2)
O(3)	0.1927 (3)	0.0539 (3)	−0.0118 (4)	2.5 (2)	2.2 (2)	10.1 (5)	1.3 (2)	−0.9 (2)	−0.3 (2)
O(4)	0.0536 (3)	0.1927 (3)	0.0122 (4)	2.2 (2)	2.6 (2)	9.4 (5)	1.3 (2)	0.1 (2)	0.7 (2)
O(5)	0.2230 (3)	0.2160 (3)	0.2121 (4)	5.9 (3)	5.2 (3)	6.3 (4)	3.6 (2)	0.1 (3)	0.5 (2)
O(6)	0.2143 (3)	0.2210 (3)	−0.2122 (4)	5.4 (3)	6.1 (3)	6.4 (4)	3.8 (3)	−0.7 (3)	−0.2 (3)
O(31)	0.2322 (3)	−0.0935 (3)	0.0207 (5)	4.5 (2)	2.7 (2)	9.6 (4)	2.4 (2)	1.6 (3)	1.1 (3)
O(41)	−0.0933 (3)	0.2320 (3)	−0.0209 (5)	3.0 (2)	4.3 (2)	9.1 (4)	2.5 (2)	−1.0 (3)	−1.4 (3)
Ow	−0.0994 (7)	−0.0560 (7)	0.0811 (9)	4.5 (5)	4.3 (5)	9.9 (9)	1.6 (4)	0.2 (6)	2.0 (6)
Ow	−0.0554 (6)	−0.0994 (8)	−0.0802 (10)	5.8 (6)	5.3 (6)	9.6 (10)	2.2 (5)	−2.4 (6)	0.1 (6)
N(5)	0.6129 (4)	0.4976 (4)	−0.0049 (4)	2.3 (2)	4.2 (3)	4.6 (4)	0.0 (2)	0.2 (2)	0.8 (3)
N(6)	0.4978 (4)	0.6125 (4)	0.0045 (4)	4.3 (3)	2.3 (2)	4.1 (4)	0.0 (2)	−0.6 (3)	−0.1 (2)
C(11)	0.4612 (5)	0.2296 (4)	0.0009 (5)	1.8 (2)	3.3 (3)	3.3 (3)	1.2 (2)	0.2 (2)	0.2 (3)
C(12)	0.4021 (4)	0.1018 (4)	0.0057 (5)	2.7 (3)	3.9 (3)	4.3 (4)	2.0 (2)	0.1 (2)	−0.2 (3)
C(13)	0.4745 (5)	0.0478 (5)	0.0090 (6)	4.5 (3)	5.7 (4)	7.3 (5)	3.9 (3)	0.5 (3)	−0.3 (4)
C(14)	0.5994 (5)	0.1132 (6)	0.0080 (7)	3.7 (3)	8.2 (5)	9.0 (6)	4.3 (3)	0.7 (4)	0.3 (5)
C(15)	0.6563 (4)	0.2375 (6)	0.0057 (6)	2.9 (3)	7.7 (5)	6.7 (6)	3.0 (3)	0.3 (3)	0.3 (4)
C(16)	0.5892 (4)	0.2969 (5)	0.0019 (5)	1.7 (2)	6.0 (4)	5.1 (4)	1.6 (3)	0.1 (2)	0.1 (3)
C(21)	0.2297 (4)	0.4611 (3)	−0.0020 (5)	3.7 (3)	1.8 (2)	3.6 (3)	1.5 (2)	0.2 (3)	0.2 (2)
C(22)	0.1019 (4)	0.4020 (4)	−0.0058 (5)	4.0 (3)	2.7 (3)	4.1 (4)	1.9 (2)	−0.1 (3)	−0.5 (2)
C(23)	0.0462 (5)	0.4731 (5)	−0.0092 (6)	5.6 (4)	4.2 (3)	7.4 (5)	3.5 (3)	−0.1 (4)	−0.4 (3)
C(24)	0.1119 (6)	0.5985 (5)	−0.0082 (7)	7.7 (5)	4.0 (3)	9.2 (6)	4.4 (3)	−0.2 (4)	−0.9 (4)
C(25)	0.2374 (6)	0.6561 (5)	−0.0046 (6)	8.0 (5)	3.2 (3)	6.6 (5)	3.4 (3)	−0.1 (4)	0.1 (3)
C(26)	0.2958 (5)	0.5888 (4)	−0.0019 (5)	6.2 (4)	1.9 (2)	4.4 (4)	1.7 (3)	0.0 (3)	−0.4 (2)
C(31)	0.2674 (4)	0.0165 (4)	0.0059 (5)	3.3 (3)	3.2 (3)	3.9 (4)	2.0 (2)	0.3 (2)	0.0 (2)
C(41)	0.0162 (4)	0.2670 (4)	−0.0057 (5)	3.1 (3)	3.8 (3)	3.8 (4)	2.3 (2)	0.4 (2)	−0.1 (2)
C(51)	0.6558 (4)	0.4253 (5)	−0.0023 (5)	2.2 (3)	5.6 (4)	4.7 (5)	0.8 (3)	−0.3 (3)	0.1 (3)
C(52)	0.6953 (5)	0.6290 (5)	−0.0185 (6)	3.6 (3)	4.8 (4)	7.8 (6)	−0.3 (3)	−0.3 (4)	1.9 (4)
C(61)	0.4254 (5)	0.6559 (4)	0.0027 (5)	5.5 (4)	2.0 (3)	4.7 (5)	0.8 (2)	−0.5 (3)	−0.1 (3)
C(62)	0.6287 (5)	0.6955 (5)	0.0183 (6)	4.8 (4)	3.1 (3)	7.7 (6)	−0.6 (3)	−2.0 (4)	0.5 (3)

atom	x	y	z	B, Å^2	atom	x	y	z	B, Å^2
H(113)	0.435	−0.040	0.014	2.7	H(151)	0.743	0.462	−0.002	2.4
H(114)	0.646	0.073	0.008	3.6	H(161)	0.462	0.743	0.004	2.3
H(115)	0.744	0.283	0.008	3.0	H(152)	0.763	0.653	0.043	3.8
H(123)	−0.041	0.423	−0.012	2.5	H(252)	0.725	0.647	−0.109	3.8
H(124)	0.071	0.645	−0.010	3.3	H(162)	0.653	0.764	−0.044	3.6
H(125)	0.283	0.744	−0.005	2.9	H(262)	0.647	0.726	0.109	3.6

(b) [CuNi]

atom	x	y	z	B_{11}	B_{22}	B_{33}	B_{12}	B_{13}	B_{23}
Cu(1)	0.44994 (4)	0.44993 (4)	0	15.1 (2)	14.8 (2)	53.9 (4)	2.1 (2)	1.2 (3)	−1.1 (3)
Ni(1)	0.21763 (3)	0.21767 (3)	−0.00030 (7)	16.5 (2)	16.6 (2)	59.5 (4)	7.4 (2)	0.9 (3)	−1.6 (3)
O(1)	0.3978 (2)	0.2832 (2)	0.0078 (4)	13 (1)	20 (1)	77 (3)	7 (1)	4 (1)	0 (2)
O(2)	0.2828 (2)	0.3972 (2)	−0.0071 (4)	19 (1)	15 (1)	80 (3)	7 (1)	−1 (2)	−4 (2)
O(3)	0.1922 (2)	0.0516 (2)	0.0096 (3)	20 (1)	15 (1)	66 (3)	10 (1)	6 (2)	1 (2)
O(4)	0.0516 (2)	0.1922 (2)	−0.0153 (3)	15 (1)	18 (1)	72 (3)	9 (1)	0 (2)	−4 (2)
O(5)	0.2129 (3)	0.2200 (3)	0.2103 (4)	39 (2)	42 (2)	54 (3)	27 (2)	−1 (2)	−6 (2)
O(6)	0.2196 (3)	0.2122 (3)	−0.2152 (4)	50 (2)	40 (2)	51 (3)	32 (2)	8 (2)	5 (2)
O(31)	0.2322 (2)	−0.0949 (2)	−0.0261 (4)	28 (2)	21 (1)	67 (3)	15 (1)	−5 (2)	−6 (2)
O(41)	−0.0945 (2)	0.2325 (2)	0.0212 (3)	21 (1)	26 (1)	62 (3)	15 (1)	5 (2)	7 (2)
Ow	−0.0549 (5)	−0.0972 (5)	0.0727 (8)	25 (5)	29 (3)	90 (8)	12 (3)	14 (4)	0 (4)
Ow	−0.0971 (5)	−0.0554 (5)	−0.0760 (8)	30 (3)	34 (4)	81 (8)	11 (3)	3 (4)	−11 (4)
N(5)	0.6165 (3)	0.4977 (3)	0.0042 (3)	16 (1)	25 (2)	37 (3)	3 (1)	2 (2)	−4 (2)
N(6)	0.4982 (3)	0.6168 (3)	−0.0104 (4)	29 (2)	16 (1)	40 (3)	4 (1)	5 (2)	−3 (2)
C(11)	0.4601 (3)	0.2273 (3)	−0.0012 (4)	14 (1)	27 (2)	30 (2)	9 (1)	2 (2)	2 (2)
C(12)	0.4020 (3)	0.0991 (3)	−0.0055 (4)	18 (2)	24 (2)	38 (3)	12 (1)	−2 (2)	0 (2)
C(13)	0.4730 (3)	0.0449 (3)	−0.0086 (4)	24 (2)	32 (2)	56 (4)	19 (2)	−5 (2)	−3 (2)
C(14)	0.5995 (3)	0.1119 (4)	−0.0051 (5)	26 (2)	49 (3)	69 (4)	26 (2)	−1 (2)	1 (3)
C(15)	0.6559 (3)	0.2356 (4)	−0.0006 (4)	18 (2)	48 (3)	48 (4)	17 (2)	−2 (2)	0 (2)
C(16)	0.5895 (3)	0.2957 (3)	0.0000 (4)	15 (1)	52 (2)	36 (3)	11 (1)	2 (2)	1 (2)
C(21)	0.2274 (3)	0.4603 (3)	−0.0048 (4)	28 (2)	13 (1)	28 (2)	10 (1)	−2 (2)	0 (2)
C(22)	0.0990 (3)	0.4022 (3)	0.0006 (4)	26 (2)	18 (2)	35 (3)	12 (1)	−2 (2)	1 (2)
C(23)	0.0450 (3)	0.4732 (3)	0.0030 (4)	35 (2)	26 (2)	53 (4)	22 (2)	−4 (2)	2 (2)
C(24)	0.1112 (4)	0.5993 (3)	−0.0011 (5)	47 (3)	27 (2)	66 (4)	26 (2)	2 (3)	7 (2)
C(25)	0.2355 (4)	0.6561 (3)	−0.0043 (4)	44 (3)	19 (2)	48 (4)	17 (2)	−1 (2)	−1 (2)
C(26)	0.2957 (3)	0.5895 (3)	−0.0060 (4)	32 (2)	16 (2)	33 (3)	10 (1)	−4 (2)	1 (2)
C(31)	0.2678 (3)	0.0148 (3)	−0.0090 (4)	20 (2)	20 (2)	32 (3)	11 (1)	−1 (2)	1 (2)
C(41)	0.0147 (3)	0.2679 (3)	0.0037 (4)	20 (2)	18 (2)	36 (3)	10 (1)	−2 (2)	0 (2)
C(51)	0.6587 (3)	0.4261 (3)	0.0038 (4)	12 (1)	30 (2)	37 (3)	3 (1)	1 (2)	0 (2)
C(52)	0.6973 (3)	0.6298 (3)	0.0143 (5)	24 (2)	26 (2)	52 (4)	−1 (2)	3 (2)	−11 (2)
C(61)	0.4258 (3)	0.6584 (3)	−0.0096 (4)	34 (2)	12 (1)	35 (3)	4 (1)	1 (2)	−1 (2)
C(62)	0.6295 (3)	0.6974 (3)	−0.0201 (4)	27 (2)	21 (2)	52 (4)	−3 (2)	10 (2)	−4 (2)

Table II (*Continued*)

atom	x	y	z	B, Å²	atom	x	y	z	B, Å²
H(113)	0.433	−0.043	−0.003	1.9	H(151)	0.746	0.462	0.021	1.6
H(114)	0.647	0.072	−0.014	2.4	H(161)	0.462	0.745	−0.007	1.7
H(115)	0.744	0.281	0.011	1.9	H(152)	0.756	0.629	−0.048	2.3
H(123)	−0.042	0.433	−0.006	1.9	H(252)	0.722	0.642	0.106	2.3
H(124)	0.071	0.647	0.017	2.4	H(162)	0.649	0.756	0.042	2.1
H(125)	0.281	0.744	−0.009	2.0	H(262)	0.642	0.722	−0.113	2.1

[a] The estimated standard deviations in the last significant figure are given in parentheses. The form of the anisotropic thermal ellipsoid is $\exp[-(\beta_{11}h^2 + \beta_{22}k^2 + \beta_{33}l^2 + 2\beta_{12}hk + 2\beta_{13}hl + 2\beta_{23}kl)]$. The B values are multiplied by 10^3.

Table III. Main Bond Lengths and Bond Angles for [NiNi] and [CuNi]

	[NiNi]	[CuNi]		[NiNi]	[CuNi]
		(a) Bond Lengths, Å			
M-O(1)	1.857 (3)	1.892 (3)	N(5)-C(51)	1.288 (8)	1.277 (5)
M-O(2)	1.851 (3)	1.896 (3)	N(5)-C(52)	1.475 (7)	1.480 (5)
M-N(5)	1.840 (4)	1.902 (3)	N(6)-C(61)	1.293 (8)	1.281 (5)
M-N(6)	1.836 (4)	1.907 (3)	N(6)-C(62)	1.471 (7)	1.472 (5)
M-Ni(1)	2.959 (1)	2.9749 (6)	C(52)-C(62)	1.517 (9)	1.539 (6)
Ni(1)-O(1)	2.010 (3)	2.022 (3)	O(1)-C(11)	1.321 (5)	1.313 (4)
Ni(1)-O(2)	2.011 (3)	2.018 (3)	O(2)-C(21)	1.321 (6)	1.316 (4)
Ni(1)-O(3)	1.971 (3)	1.986 (3)	O(3)-C(31)	1.275 (5)	1.286 (4)
Ni(1)-O(4)	1.975 (3)	1.989 (3)	O(4)-C(41)	1.271 (5)	1.286 (4)
Ni(1)-O(5)	2.109 (4)	2.069 (3)	C(51)-C(16)	1.421 (8)	1.448 (5)
Ni(1)-O(6)	2.112 (4)	2.111 (3)	C(61)-C(26)	1.434 (8)	1.445 (5)
O(1)-O(2)	2.481 (4)	2.541 (3)	C(31)-C(12)	1.507 (6)	1.506 (4)
O(1)-O(3)	2.828 (4)	2.815 (3)	C(41)-C(22)	1.510 (6)	1.506 (4)
O(1)-O(5)	2.909 (5)	2.921 (4)	C(31)-O(31)	1.252 (5)	1.249 (4)
O(1)-O(6)	2.936 (5)	2.914 (5)	C(41)-O(41)	1.246 (5)	1.248 (4)
O(1)-N(5)	2.704 (5)	2.774 (4)	C(11)-C(12)	1.416 (6)	1.424 (4)
O(2)-O(4)	2.835 (5)	2.810 (3)	C(12)-C(13)	1.403 (6)	1.393 (4)
O(2)-O(5)	2.829 (5)	2.911 (4)	C(13)-C(14)	1.382 (7)	1.404 (5)
O(2)-O(6)	2.919 (6)	2.920 (4)	C(14)-C(15)	1.376 (9)	1.375 (6)
O(2)-N(6)	2.699 (5)	2.786 (4)	C(15)-C(16)	1.401 (8)	1.404 (5)
O(3)-O(4)	3.081 (5)	3.128 (3)	C(16)-C(11)	1.416 (8)	1.436 (4)
O(3)-O(5)	2.929 (6)	2.834 (4)	C(21)-C(22)	1.414 (6)	1.427 (5)
O(3)-O(6)	2.830 (6)	2.915 (4)	C(22)-C(23)	1.407 (6)	1.391 (4)
O(4)-O(5)	2.841 (5)	2.926 (4)	C(23)-C(24)	1.387 (7)	1.400 (5)
O(4)-O(6)	2.928 (6)	2.827 (4)	C(24)-C(25)	1.389 (9)	1.380 (5)
N(5)-N(6)	2.546 (6)	2.635 (4)	C(25)-C(26)	1.392 (8)	1.407 (5)
			C(26)-C(21)	1.413 (6)	1.433 (4)
		(b) Bond Angles, Deg			
N(5)-M-O(1)	94.0 (2)	94.0 (1)	O(1)-Ni(1)-O(6)	90.8 (2)	89.6 (1)
O(1)-M-O(2)	84.0 (1)	84.2 (1)	O(2)-Ni(1)-O(3)	166.5 (1)	167.1 (1)
O(2)-M-N(6)	94.2 (2)	94.2 (1)	O(2)-Ni(1)-O(4)	90.7 (1)	89.1 (1)
N(6)-M-N(5)	87.7 (2)	87.5 (1)	O(2)-Ni(1)-O(5)	90.6 (2)	90.8 (1)
M-O(1)-Ni(1)	99.8 (2)	98.9 (1)	O(2)-Ni(1)-O(6)	90.1 (2)	90.0 (1)
M-O(2)-Ni(1)	99.8 (2)	98.9 (1)	O(3)-Ni(1)-O(4)	102.7 (1)	103.8 (1)
O(1)-Ni(1)-O(2)	76.2 (1)	77.9 (1)	O(3)-Ni(1)-O(5)	91.7 (2)	88.6 (1)
O(1)-Ni(1)-O(3)	90.5 (1)	89.2 (1)	O(3)-Ni(1)-O(6)	87.7 (2)	90.7 (1)
O(1)-Ni(1)-O(4)	166.7 (1)	166.6 (1)	O(4)-Ni(1)-O(5)	88.1 (2)	92.3 (1)
O(1)-Ni(1)-O(5)	89.9 (2)	91.1 (1)	O(4)-Ni(1)-O(6)	91.4 (2)	87.1 (1)
			O(5)-Ni(1)-O(6)	179.2 (4)	179.0 (3)

had already been performed. The data presented here are more accurate than those already published.[27] When the complex is cooled down from 300 to about 60 K, $\chi_M T$ decreases, then reaches a plateau defined by $\chi_M T = 0.52$ (0) cm^3 mol^{-1} K, and finally decreases again below 16 K. Qualitatively, this magnetic behavior may be easily explained: the $^2A_1$ state is the lowest. Below 60 K, the $^4A_1$ excited state is totally depopulated, so that the magnetic susceptibility follows the Curie law expected for a spin doublet. The decrease of $\chi_M T$ below 16 K, already observed in [CuMg] and [NiNi], may be again attributed to intermolecular interactions.

The appropriate spin Hamiltonian to describe the low-lying states in [CuNi] may be written

$$\mathcal{H} = \beta H(\mathbf{g}_{Cu}\cdot\hat{S}_{Cu} + \mathbf{g}_{Ni}\cdot\hat{S}_{Ni}) + \hat{S}_{Ni}\cdot\mathbf{D}\cdot\hat{S}_{Ni} - J\hat{S}_{Cu}\cdot\hat{S}_{Ni} + \hat{S}_{Cu}\cdot\mathbf{D}_{CuNi}\cdot\hat{S}_{Ni} \quad (1)$$

where the first two terms are the single-ion Zeeman perturbations, the third term is the local zero-field splitting around the Ni^{II} ion, the fourth term is the isotropic exchange, and the last term is the anisotropic exchange. The Dzyaloshinsky term of the form $d_{CuNi}\cdot\hat{S}_{Cu} \wedge \hat{S}_{Ni}$ is zero because the two metal sites and the whole molecule have a C_{2v} symmetry, with coincident symmetry axes.[28] The *status* of this Hamiltonian will be discussed further on. Here, we restrict ourselves to the derivation of the magnetic susceptibility from (1).

We have seen that up to around 60 K, only the $^2A_1$ state is populated. This indicates that the separation $3J/2$ between $^2A_1$ and $^4A_1$ is large with regard to the eventual zero-field splitting of $^4A_1$. It turns out that the influence of this zero-field splitting on the magnetic behavior may be neglected. The derivation of the molar magnetic susceptibility then leads to[29]

(27) Tola, P.; Kahn, O.; Chauvel, C.; Coudanne, H. *Nouv. J. Chim.* **1977** *1*, 467.

(28) Moriya, T. *Magnetism* **1963**, *1*, 85.

(29) Griffith, J. S. *Struct. Bonding (Berlin)* **1972**, *10*, 87.

$$\chi_M = \frac{N\beta^2}{4kT}\frac{\bar{g}_{1/2}^2 + 10\bar{g}_{3/2}^2 \exp(3J/2kT)}{1 + 2\exp(3J/2kT)} - \frac{8\beta^2\delta^2}{3J}\frac{1 - \exp(3J/2kT)}{1 + 2\exp(3J/2kT)} \quad (2)$$

with

$$\mathbf{g}_{1/2} = \mathbf{g}_{Ni} - \delta \qquad \mathbf{g}_{3/2} = \mathbf{g}_{Ni} + \delta \qquad \delta = (\mathbf{g}_{Cu} - \mathbf{g}_{Ni})/3 \quad (3)$$

$\mathbf{g}_{1/2}$ and $\mathbf{g}_{3/2}$ are the g tensors associated to the doublet and quartet states, respectively, and $\bar{g}_{1/2}$ and $\bar{g}_{3/2}$ the average g factors. The second term in (2) is due to the coupling of the $M_S = \pm^1/_2$ components arising from each of these two states. In fact, we determined that this second-order term does not play any significant part in the magnetic properties of [CuNi], owing to the large $^2A_1$–$^4A_1$ separation.

Taking into account a TIP of 110×10^{-6} cm^3 mol^{-1} for the Ni^{II} ion, i.e., the half of the TIP found in [NiNi], we determined J and the average values $\bar{g}_{1/2}$ and $\bar{g}_{3/2}$ by a least-squares procedure in the temperature range 300–16 K and found

$$J = -142 \text{ cm}^{-1} \qquad \bar{g}_{1/2} = 2.35\ (4) \qquad \bar{g}_{3/2} = 2.21$$

The agreement factor defined by $\sum T^2(\chi_M(\text{obsd}) - \chi_M(\text{calcd}))^2/\sum T^2\chi_M(\text{obsd})^2$ is then equal to 2×10^{-5}. Experimental data and the calculated curve are compared in Figure 5. One can notice here that if the two g factors are supposed to be identical, the agreement factor is significantly less good, namely, 6×10^{-4}, and J is then found equal to -161 cm^{-1}.

EPR Spectra. The powder spectrum of [CuMg] at 4 K is typical of an isolated Cu^{II} ion in an axial surrounding; the principal g values are $g_\parallel = 2.13$ and $g_\perp = 2.06$ (see Figure 6).

The powder spectrum of [NiNi] at 4 K only exhibits signals of very weak intensity, so that most likely they do not belong to the actual product. These signals could be due to a Ni^{II} impurity in a surrounding more symmetrical than the outside Ni^{II} of the [NiNi] molecule.

The powder spectrum of [CuNi] at 4 K is shown in Figure 6. It is typical of an axial symmetry yielding the principal values $g_\parallel = 2.20$ (4) and $g_\perp = 2.28$. The comparison with [CuMg] unambiguously shows that this spectrum results from the interaction and belongs to the ground doublet state put in evidence by the magnetic behavior. Indeed, at 4 K, the excited quartet state is completely depopulated.

The single-crystal spectra of [CuNi] were recorded with the static magnetic field in three orthogonal planes, one of the planes being perpendicular to the crystal unique axis (c axis). At 4 K, only one signal is observed for any orientation of the crystal, assigned to the ground-pair doublet state. The angular dependence (Figure 7) and the principal $g_{1/2}$ values show that, at the accuracy of the experimental measurements, the $\mathbf{g}_{1/2}$ tensor is axial with $g_{1/2_\parallel}$ along the c axis equal to 2.22 (5) and $g_{1/2_\perp}$ equal to 2.30 (0). The intramolecular Cu–Ni directions and the mean planes of the macrocycles are perpendicular to the c axis (see above). It turns out that $\mathbf{g}_{1/2}$ is isotropic in the $N_2CuO_2NiO_2$ pseudo molecular plane. Such an isotropy in a macrocycle plane was already pointed out by one of us in seven-coordinate complexes.[30]

The line width is both orientation and temperature dependent. It is minimal when the magnetic field is along the c axis. When the temperature increases, the broadening is inhomogeneous, being more pronounced on the high-field side of the signal for all the orientations but with the magnetic field along the c axis. At the high-field side, around 3300 G, a badly resolved and weak feature is observed, the intensity of which is maximum when the magnetic field is perpendicular to the c axis. Two assignments for this feature could be considered: either it arises from the excited quartet state or it belongs to an impurity. For some orientations, this feature appears at

(30) Gerloch, M.; Morgenstern-Badarau, I. *Inorg. Chem.* **1979**, *18*, 3225.

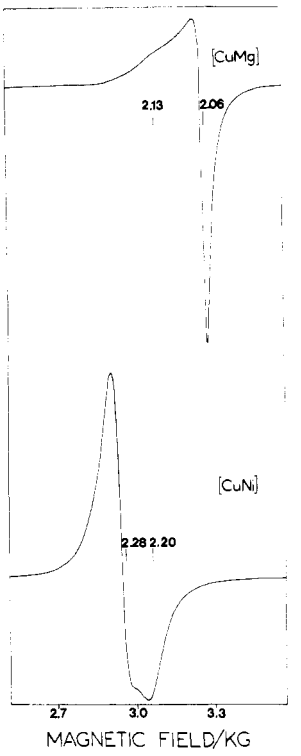

Figure 6. Powder X-band EPR spectra of [CuMg] and [CuNi].

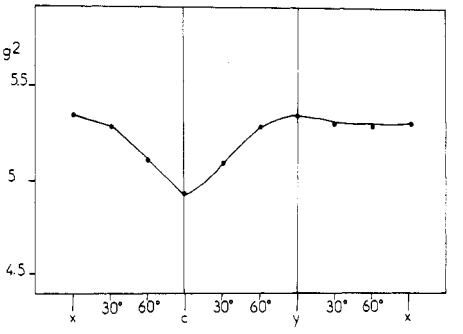

Figure 7. Angular dependence of the g^2 values in two orthogonal planes (zx and zy) for [CuNi] at 4 K.

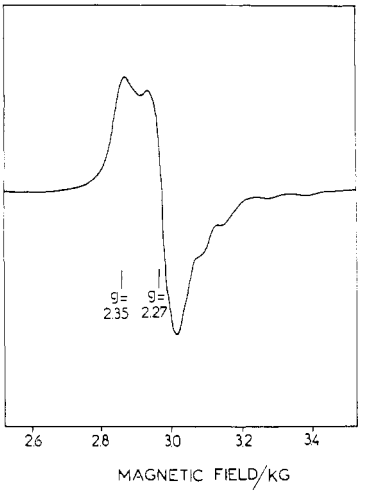

Figure 8. Glass X-band EPR spectrum of [CuNi] in 90% methanol–10% ethanol.

Table IV. Mean Planes

Mean Planes

A defined by O(1)O(2)N(5)N(6)
B defined by O(1)O(2)O(3)O(4)
C defined by M[a]Ni(1)O(5)O(6)

Dihedral Angles, Deg

	[NiNi] (1)	[CuNi] (2)		[NiNi] (1)	[CuNi] (2)
A–B	178.5	178.8	B–C	88.8	88.6
A–C	90.3	90.7			

Deviations of the Atoms from Mean Planes ($\times 10^3$), Å

	A		B		C	
atoms	1	2	1	2	1	2
M	−3 (1)	−27 (1)	−6 (1)	−25 (1)	0 (1)	0 (1)
Ni(1)	−6 (1)	−21 (1)	−1 (1)	−24 (1)	0 (1)	0 (1)
O(1)	−5 (4)	11 (4)	−39 (4)	37 (4)	1242 (4)	1271 (3)
O(2)	5 (4)	−11 (4)	38 (4)	−37 (4)	−1239 (4)	−1271 (3)
O(3)	65 (4)	−50 (3)	31 (4)	−23 (3)	1538 (4)	1562 (3)
O(4)	−79 (4)	60 (3)	−31 (4)	23 (3)	−1542 (4)	−1564 (3)
O(5)	−2114 (4)	−2090 (4)	−2110 (4)	−2092 (4)	2 (4)	−1 (4)
O(6)	2106 (4)	2090 (4)	2110 (4)	2086 (4)	−2 (4)	1 (4)
N(5)	8 (4)	−14 (3)	−33 (4)	18 (3)	1278 (5)	1318 (4)
N(6)	−8 (4)	16 (4)	19 (4)	−6 (4)	−1268 (5)	−1318 (4)

[a] In 1 M = Ni; in 2 M = Cu.

temperatures as low as 4 K, which is inconsistent with a quartet state located at 213 cm^{-1} above the ground doublet state. This strongly suggests that the second hypothesis was the right one.

The glass spectrum at 4 K is given in Figure 8. It exhibits two main signals with $g_1 = 2.35$ (4) and $g_2 = 2.27$ and four unequally spaced and weakly intense features in the high-field region. Two alternative interpretations can be proposed: (i) Considering the whole spectrum, we may think of a rhombic symmetry with an hyperfine structure for the pair state. In such a case, we have $g_3 = 2.09$. It may be pointed out that only the g_2 component for [CuNi] in the glass sample is in good agreement with one of the principal values of the $\mathbf{g}_{1/2}$ tensor obtained in solid state. That supposes that the molecular symmetry in solution is different from the symmetry in the solid state. Maybe a methanol molecule is weakly bound to the Cu^{II} ion as observed in many $CuM(fsa)_2en$ complexes.[2,26] (ii) The weak signals could be due to a Cu^{II} impurity with a $g_\perp$ value of 2.09, very close to that observed in [CuMg]. The two main peaks would be therefore assigned to the axial and perpendicular components of the $\mathbf{g}_{1/2}$ tensor for [CuNi].

Discussion

In this section, we shall approach the three following points: (i) The *status* of the Hamiltonian (1); (ii) the comparison of the magnetic and EPR results; (iii) the mechanism of the exchange in [CuNi].

Status of the Hamiltonian (1). The spin Hamiltonians associated with the $S = {}^1/_2$ and $S = {}^3/_2$ states may be written as

$$\mathcal{H}_{1/2} = \beta H \cdot \mathbf{g}_{1/2} \cdot \hat{S} \qquad \mathcal{H}_{3/2} = \beta H \cdot \mathbf{g}_{3/2} \cdot \hat{S} + \hat{S} \cdot \mathbf{D} \cdot \hat{S} \qquad (4)$$

where the parameters may be deduced from those of (1) according to the relations (3) for the $\mathbf{g}_{Cu}$, $\mathbf{g}_{Ni}$, $\mathbf{g}_{1/2}$, and $\mathbf{g}_{3/2}$ tensors and the relation (5) for the $\mathbf{D}_{Ni}$, $\mathbf{D}_{NiCu}$, and $\mathbf{D}$ tensors.[6] Some

$$\mathbf{D} = (\mathbf{D}_{Ni} + \mathbf{D}_{CuNi})/3 \qquad (5)$$

of the approximations considered when (1) and (4) are written out have already been specified;[31,32] (4) is valid only when $-J\hat{S}_{Cu} \cdot \hat{S}_{Ni}$ is the leading term in (1), in order for $S = {}^1/_2$ and $S = {}^3/_2$ to be good quantum numbers. Moreover (4) holds because the Cu^{II} and Ni^{II} interacting ions are orbital singlets without first-order angular momentum. However, in our opinion, to keep in mind these approximations is far from being enough to understand what is the actual *status* of (1). In fact, the spin Hamiltonian (1) implicitly requires that the wave functions of the real electrostatic Hamiltonian describing the low-lying pair states have the form of Heitler–London functions constructed from eigenfunctions of local Hamiltonians. In the same way, it is implicitly assumed that the coupling between the ground configuration $Cu^{II}Ni^{II}$ and the excited configurations where an electron is transferred from one ion to the other ($Cu^{III}Ni^{I}$ or $Cu^{I}Ni^{III}$) is negligible. It should be emphasized that these approximations are exactly the same as those used to build an orbital model of the exchange.[28,33,34] Therefore, one may think that the verification of the relations (3) for a given compound could be a proof of the validity of our model for this compound. In contrast, the nonverification of (3) could indicate the limits of this model. In particular, we already noticed that our model became deficient for very strong antiferromagnetic interactions.[14] It would be very interesting to specify when the interaction is too strong in order for the orbital model to be valid.

Comparison of the Magnetic and EPR Results. The EPR gives accurate principal values for the $\mathbf{g}_{1/2}$ tensor and thus an accurate average value $\bar{g}_{1/2}$. The Curie law observed in magnetism between 60 and 16 K should also lead to a good determination of $\bar{g}_{1/2}$. The two values obtained are 2.27 (4) (EPR) and 2.35 (4) (magnetism). The agreement is far from being excellent. The error in magnetism arises from the uncertainties of the method, namely, the standardizing, the weighings, the chemical purity, and the correction of diamagnetism. The errors in weighing and in standardizing affect all the experimental data of a constant factor and therefore show up in the g values. The diamagnetic correction error is certainly small and only affects the highest temperatures and not the plateau of χT between 60 and 16 K. As for the eventual presence of a few parts per million of foreign metallic ions, its effect cannot be predicted a priori. For [CuMg], where in the whole temperature range a Curie law is observed, the EPR–magnetism agreement is better, with $\bar{g}_{Cu} = 2.08$ and 2.11, respectively. On the other hand, for [NiNi] only the

(31) Buluggiu, E.; Vera, A. *Z. Naturforsch., A* **1976**, *31A*, 911; *J. Magn. Reson.* **1980**, *41*, 195.
(32) Chao, C. C. *J. Magn. Reson.* **1973**, *10*, 1.
(33) Girerd, J. J.; Charlot, M. F.; Kahn, O. *Mol. Phys.* **1977**, *34*, 1063.
(34) Kahn, O.; Charlot, M. F. *Nouv. J. Chim.* **1980**, *4*, 567.

magnetism allows us to obtain $\bar{g}_{Ni}$.

As far as the excited quartet state in [CuNi] is concerned, we do not observe EPR signals, even above 60 K where the magnetism indicates that the quartet state is populated. This suggests that the signals associated with $S = {}^3/_2$ are hidden, at least in part, by the intense single peak associated with $S = {}^1/_2$. We noticed that, when the temperature increases, the broadening of this peak on the high-field side (thus smaller g) was more pronounced than that on the low-field side. This dissymmetry in the line width could be due to the presence of resonances in the quartet state. This broadening is minimal for the magnetic field along the c axis. For this orientation, the main peak in $S = {}^3/_2$ would be located very close to the peak $S = {}^1/_2$, i.e., for $\bar{g}_{3/2} \simeq 2.22$. In magnetism, we obtain $\bar{g}_{3/2} = 2.21$.

The main characteristic of the exchange is the energy gap $3J/2$ between doublet and quartet states. The temperature dependence of the magnetic susceptibility most likely leads to an accurate value of this gap, namely, -213 cm^{-1}. One will notice that the agreement between theory and experimental data is excellent, compared to that of other systems investigated in our group. This doublet–quartet energy gap could be in principle deduced from the study of the EPR intensities. In the 4–60 K temperature range, the product intensity times the temperature is constant, confirming the Curie law observed in magnetism when only the ground doublet state is populated. Above 60 K, unfortunately, the inhomogeneous broadening leads to a large uncertainty of the intensity measurements.

Let use examine now the relations (3). We obtained $\bar{g}_{Cu}$ and $\bar{g}_{Ni}$ from the magnetic data for [CuMg] and [NiNi], respectively. $\bar{g}_{1/2}$ and $\bar{g}_{3/2}$ may be obtained from the magnetic data for [CuNi] or calculated from (3):

	exptl	calcd
$\bar{g}_{Cu}$	2.11	
$\bar{g}_{Ni}$	2.29	
$\bar{g}_{1/2}$	2.35 (4)	2.35
$\bar{g}_{3/2}$	2.21	2.23

The agreement may appear quite satisfying. Owing to the uncertainties of the g values determined in magnetism, this agreement may even be to some extent fortuitous. In EPR, we only obtained two certain values, namely, $\bar{g}_{1/2}$ and $\bar{g}_{Cu}$, and therefore we cannot test the relations (3). It turns out that in the present case the validity of the relations (3) remains an open problem.

Mechanism of the Exchange. In this section, we shall use theoretical concepts developed in our group for several years without rederiving them. We consider that only the three magnetic electrons are active electrons and write the electrostatic Hamiltonian according to

$$\mathcal{H} = \sum_{i=1}^{3} h(i) + \sum_{i}\sum_{j>i} 1/r_{ij} \qquad (6)$$

$h(i)$ is the monoelectronic Hamiltonian acting on the electron i and r_{ij} is the interelectronic distance. In absence of interaction, the unpaired electron around Cu^{II} is described by an xy type orbital of b_1 symmetry, denoted $b_1(Cu)$, and the two unpaired electrons around Ni^{II} are described by xy and z^2 type orbitals of b_1 and a_1 symmetry, respectively, denoted $b_1(Ni)$ and $a_1(Ni)$. These orbitals are schematically represented in Figure 9. The isotropic exchange interaction parameter J may be decomposed according to

$$J = {}^1/_2(J_{b_1a_1} + J_{b_1b_1}) \qquad (7)$$

Taking the wave functions associated to the $^2A_1$ and $^4A_1$ low-lying states as Heitler–London functions constructed from the magnetic orbitals $b_1(Cu)$, $b_1(Ni)$, and $a_1(Ni)$ and expanding the eigenvalues of $\mathcal{H}$ according to the increasing

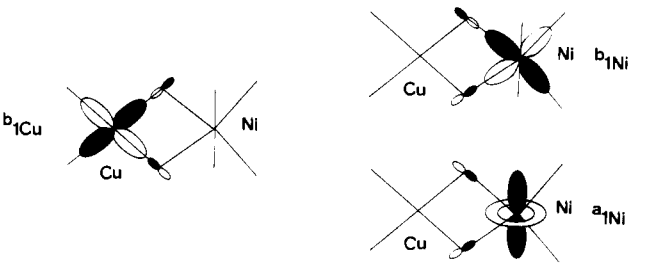

Figure 9. Magnetic orbitals centered on Cu^{II} and Ni^{II} in [CuNi].

powers of the overlap integrals between magnetic orbitals, one obtains[35]

$$J_{\mu\nu} = 4t_{\mu\nu}S_{\mu\nu} + 2j_{\mu\nu} + \text{terms in } S_{\mu\nu}{}^2\ldots$$

with

$$t_{\mu\nu} = \left\langle \mu_{Cu}(i)\left|h(i) - \frac{(\alpha\mu_{Cu} + \alpha\nu_{Ni})}{2}\right|\nu_{Ni}(i)\right\rangle$$
$$\alpha\mu_{Cu} = \langle\mu_{Cu}(i)|h(i)|\mu_{Cu}(i)\rangle \qquad S_{\mu\nu} = \langle\mu_{Cu}(i)|\nu_{Ni}(i)\rangle \qquad (8)$$
$$j_{\mu\nu} = \langle\mu_{Cu}(i)\nu_{Ni}(j)|r_{ij}^{-1}|\mu_{Cu}(j)\nu_{Ni}(i)\rangle$$

The $b_1(Cu)$ and $a_1(Ni)$ orbitals are orthogonal, so that one has

$$J_{b_1a_1} = 2j_{b_1a_1} > 0$$

$J_{b_1a_1}$ is then a ferromagnetic contribution, contrary to what was recently asserted.[8] Owing to the weak delocalization of $a_1(Ni)$ toward the bridging oxygen atoms, $J_{b_1a_1}$ may be expected to be weakly ferromagnetic. In contrast, $J_{b_1b_1}$ defined as

$$J_{b_1b_1} = 4t_{b_1b_1}S_{b_1b_1} + 2j_{b_1b_1}$$

has a negative contribution due to the nonorthogonality of the magnetic orbitals. $4t_{b_1b_1}S_{b_1b_1}$ may be reexpressed according to $2(\Delta_{b_1b_1}{}^2 - \delta_{b_1b_1}{}^2)^{1/2}S_{b_1b_1}$, where $\delta_{b_1b_1}$ is the energy gap between the two magnetic orbitals and $\Delta_{b_1b_1}$ the energy gap between the two molecular orbitals build from $b_1(Cu)$ and $b_1(Ni)$ in the state of highest spin multiplicity ($S = {}^3/_2$),[28] as shown in II.

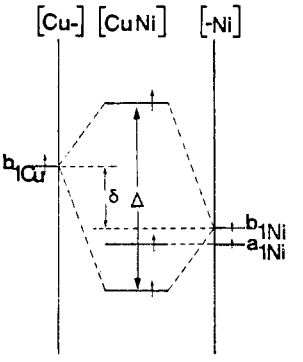

II

The magnitude of $J_{b_1b_1}$ in a

bridging network according to the nature of the bridges X and of the structural parameters was theoretically and experimentally discussed by several authors.[14,34,36,37] It is enough

(35) Girerd, J. J. Thesis, Université Paris-Sud, 1981.
(36) Hay, P. J.; Thibeault, J. C.; Hoffmann, R. *J. Am. Chem. Soc.* **1975**, *97*, 4884.
(37) Crawford, V. H.; Richardson, H. W.; Wasson, J. R.; Hodgson, D. J.; Hatfield, W. E. *Inorg. Chem.* **1976**, *15*, 2107.

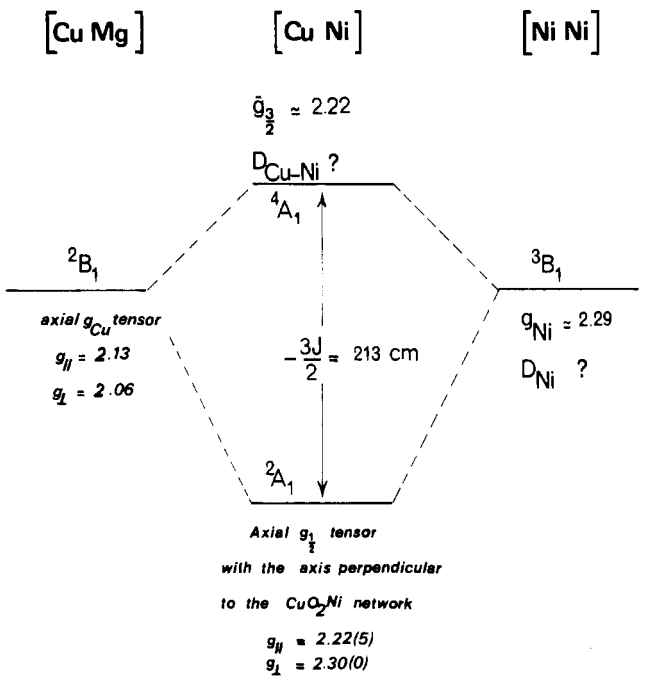

Figure 10. Schematic representation of the electronic structure of the low-lying states in [CuNi]. The information deduced from magnetism are written in boldface characters; those deduced from EPR are written in italics.

to recall here that for bridging angles of 99° and a planar network, $J_{b_1b_1}$ is expected to be strongly antiferromagnetic. Consequently, one conceives that, in spite of the $J_{b_1a_1}$ contribution, the observed coupling is largely antiferromagnetic.

Conclusion

The classical techniques of the crystallography led to an accurate description of the molecular structure of [CuNi], represented in Figure 2. In a similar way, the two complementary techniques magnetism and EPR gave us a relatively accurate description of the two low-lying states in this complex, as is represented in Figure 10, where we used different characters to note the information deduced from magnetism and that deduced from EPR. We also specified the information we were not able to obtain, essentially the structure of the excited $^4A_1$ state in [CuNi]. This difficulty encountered in this work concerning the quartet state appears inherent in the studied compound. This is why we propose to investigate other $Cu^{II}Ni^{II}$ complexes with the hope of encountering favorable cases where all the expected information could be derived.

As far as the mechanism of the exchange is concerned, the leading phenomenon of isotropic exchange is now qualitatively rather well understood. In [CuNi], there are two pathways, $J_{b_1b_1}$ and $J_{b_1a_1}$. The dominant pathway $J_{b_1b_1}$ is antiferromagnetic while the $J_{b_1a_1}$ pathway involving orthogonal magnetic orbitals is ferromagnetic. In contrast, much still remains to be done as regards the mechanism of the anisotropic exchange. It is well established that the anisotropic exchange is due to the combined effect of the spin–orbit coupling and the isotropic exchange.[29] However, no orbital model has been proposed. Our laboratory is working in this direction.

Acknowledgment. We are most grateful to J. L. Brayer, J. Livage, and C. Sanchez for their help in recording some of the EPR spectra and for stimulating discussions. We also acknowledge J. Ammeter and D. Gatteschi for their critical reading of the manuscript.

Registry No. [CuNi], 81737-74-8; [CuMg], 70296-15-0; [NiNi], 81737-75-9.

Supplementary Material Available: Listings of structure factor amplitudes and root-mean-square amplitudes of vibration (43 pages). Ordering information is given on any current masthead page.